Actinic Inspection of the EUV Optical Parameters of Lithographic Materials with Lab-Based Radiometry and Reflectometry

Kevin M. Dorney[a,*], Nicola N. Kissoon[b], Fabian Holzmeier[a], Esben W. Larsen[a],
Dhirendra P. Singh[a], Shikhar Arvind[a,c], Sayantani Santra[a,c], Roberto Fallica[a],
Igor Makhotkin[d], Vicky Philipsen[a], Stefan De Gendt[a,c], Claudia Fleischmann[a,b],
Paul A.W. van der Heide[a], John S. Petersen[a]

[a]imec, Kapeldreef 75, 3001 Leuven, Belgium
[b]Quantum Solid State Physics, KU Leuven, Celestijnenlaan 200d, 3001 Leuven, Belgium
[c]Chemistry Department, KU Leuven, Celestijnenlaan 200f, 3001 Leuven, Belgium
[d]Industrial Focus Group XUV Optics, MESA+ Institute for Nanotechnology, University of Twente, Drienerlolaan 5, 7522 NB Enschede, The Netherlands

ABSTRACT

The interaction of EUV light with matter is a critical step in EUV lithographic processes and optimization of the optical material parameters of photoresists and reflector/absorber stacks is crucial to harness the full power of EUV lithography. To optimize these materials, accurate measurements of EUV absorption and reflection are needed to extract the corresponding actinic optical properties and structural parameters. Here, we report on two endstations within imec's AttoLab that enable actinic EUV absorption and reflection measurements. We commission these tools with measurements on model thin film and photoresist systems and provide extracted optical parameters as well as absorption kinetics, respectively. These results showcase the power of these tools for providing crucial data for material optimization and lithographic simulation.

Keywords: EUV, EUV lithography, photoresists, reflectometry, absorption coefficient, Dill parameters, thin films, interfaces, optical constants

1. INTRODUCTION

As the semiconductor industry adapts to extreme ultraviolet (EUV) lithography in high-volume manufacturing (HVM), novel materials (e.g., reflectors, absorbers, photoresists) are continually being evaluated for their performance at the actinic wavelength of 13.5 nm. Crucial to the implementation, optimization, and simulation of these EUV-responsive materials is an accurate determination of optical parameters, as the light-matter interaction governed by these parameters contributes largely to their performance in EUV lithography systems. Moreover, the direct relationships between optical constants and material structure/chemistry provide a means of correlating optical response to material design, thus opening a path for data-driven optimization of novel EUV material candidates. As such, significant effort has been put forth in recent years to develop methodologies that can measure both optical constants and material parameters at the actinic wavelength of 13.5 nm. These techniques, typically based on reflection/scatterometry [1-5] or transmission measurements [6-9], have provided crucial optical data on "real-world" material systems that aid in characterization of their fundamental properties.

The optical response of a material to EUV light is governed by its complex refractive index, $\tilde{n}$, approximated by $\tilde{n}=n + ik = 1 - \delta + i\beta$ and comprised of dispersive (n or $1-\delta$) and absorptive parts (k or β). These so-called "optical constants" play an important role in the performance of EUV materials. For instance, the absorption of EUV light by photoresists (determined by their β parameter) depends heavily on their composition. Increasing the absorption properties of EUV resists (via compositional changes) enables lower exposure doses and faster processing speeds. Indirectly, a higher absorption coefficient for a photoresist can also result in a larger number of primary electrons being produced (and possibly also secondary electrons), which in turn will enhance the resist sensitivity. These effects have led to a large effort in recent years to increase the absorptivity of photoresists, such as the addition of elements with high EUV absorption cross-section (e.g., Zr or Hf) in CAR-based systems, or by moving to MOR platforms that directly contain highly absorbing metals (e.g.,

Sn) in the resist structure [10]. While EUV absorption can be calculated from individual absorption cross-sections [11], these simulations rely on database values that often differ from experimental values on real thin films [7, 8], particularly near resonance features or in regions where data is incomplete [12]. While EUV transmission measurements give direct access to the resist absorptivity, these techniques have been primarily limited to synchrotron facilities, which presents a bottleneck for rapid characterization of new resist platforms.

Aside from photoresists, new materials are continually being evaluated for use in EUV optics and imaging, which places a high interest on measuring the optical constants that drive their performance. Novel alloys are being explored for use in alternative EUV masks designs that can aid in improving the imaging process, especially for technology nodes supported by the upcoming high-NA EUV ecosystem. Compound alloys (e.g., RuTa [13], TaTeN [14], etc.) are being explored as a new class of absorber materials to enable EUV versions of binary and phase-shifting masks, yet evaluating these material candidates requires rigorous modelling of their imaging properties. These simulations in turn require accurate optical parameters, which has motivated the development of inspection methods to obtain these parameters from "real-world" systems. EUV reflectometry has emerged as a powerful technique that can extract not only optical but also material properties from thin film systems. Moreover, this technique can be applied to both hard [1,2,13,14] and soft matter [3,4,15] alike, opening a wide range of material classes that can be characterized. However, EUV reflectivity measurements require high-brightness EUV sources that are also typically available from synchrotron facilities with limited beamtime and accessibility.

In this work, we present recent developments within imec's AttoLab [16] to develop actinic EUV absorption (radiometry) and reflectometry capabilities from a tabletop, accessible EUV system. To realize these capabilities, we have constructed two separate endstations enabling, separately, EUV absorption studies on transparent EUV materials and EUV reflectivity measurements on thin films and stacks. We leverage these techniques to characterize the optical and structural properties of model EUV photoresists and thin films, which enables extraction of absorption coefficients and n and k values. Moreover, we show the sensitivity of EUV reflectometry to quantify interfacial formation and diffusion. Additionally, we compare our results to those obtained by recent synchrotron experiments, which further validates the capability of lab-based actinic inspection methods to characterize EUV materials.

2. EXPERIMENTAL METHODS

Actinic EUV absorption and reflection measurements are performed in imec's AttoLab, an ultrafast materials characterization and EUV interference lithography laboratory [16]. The lab is driven by two ultrafast EUV sources based on high-harmonic generation (HHG), which provide highly coherent and bright EUV light for spectroscopic or lithographic applications. A detailed description of the EUV sources as well as the radiometry and reflectometry endstations are given below.

2.1 Ultrafast, coherent EUV sources in imec's AttoLab

The various beamlines in imec's AttoLab are supplied by HHG-based EUV systems, which provide bright, highly coherent, and ultrashort pulsed EUV radiation in the range of 30 – 55 eV or 75 – 120 eV (depending on the application). A commercial Ti:sapphire amplifier (KM Labs RAEA™) produces femtosecond near-infrared (IR) pulses (2.6 mJ, 25fs, 5 kHz, 790 nm) that are then used to drive the HHG process in a commercial HHG system (KM Labs XUUS 4™). For radiometry and reflectometry experiments, He gas is used as the generating medium, which yields a bright, coherent EUV beam with a broad, comb-like spectrum centered around 13.5 nm (inset Figure 1). Following the HHG system, a pair of grazing-incidence reflections on Ru-coated mirrors serve to remove >99% of the driving near-IR beam while also enabling pointing control of the EUV light. A pair of Zr metal foil filters (150 nm thickness) then serve to remove the remaining near-IR light, as well as to remove lower-order UV/VUV light from the HHG process. Following the Zr filters, a set of mirrors on a motorized translation stage allows for sending the EUV beam to either the radiometry (Section 2.2) or reflectometry endstations (Section 2.3).

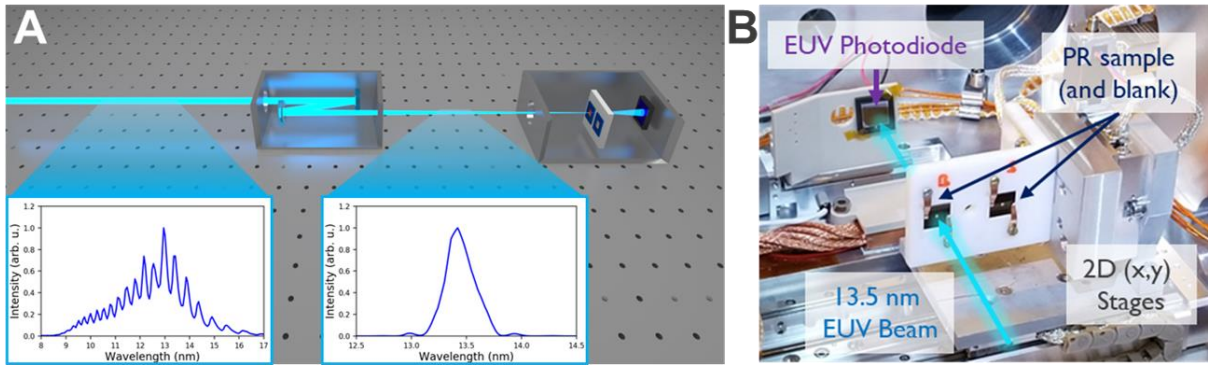## 2.2 AttoLab's Actinic EUV Radiometry Endstation

Figure 1. (A) Schematic of the radiometry beamline in imec's AttoLab, depicting the monochromator chamber, which serves to both focus the EUV beam and spectrally select the 13.5 nm harmonic from the broad harmonic comb (insets). (B) Photograph of the radiometry endstation sample chamber, showing the sample holder, positioning stages, and EUV photodiode.

The radiometry endstation is installed on AttoLab's spectroscopy beamline and is comprised of a vacuum chamber with an EUV sensitive photodiode detector (AXUV100G, OptoDiode) and a 2D translation stage for mounting resist-coated and "blank" Si_3N_4 membranes (Figure 1b). Prior to this endstation, the EUV light emerging from the HHG system is spectrally filtered by a pair of MoSi multilayer mirrors (6-deg incidence angle, NTT-AT), yielding a femtosecond EUV beam at 13.5 nm ($\Delta\lambda/\lambda \sim 1.4 \times 10^{-2}$). The final MoSi mirror (f=50 cm) in the monochromator chamber also serves to focus the EUV beam onto the sample, resulting in a spot size of ~30 µm x 30 µm ($1/e^2$ radius). This leads to an on-target photon flux of ~5×10^8 photons/sec and a writing speed of ~0.19 $mJ/cm^2/s$ @ 13.5 nm, with a flux stability of <3% RMS over several hours of operation. Actinic exposures of the photoresist are performed in a 3 x 3 grid pattern, with the outer positions of the grid corresponding to "short" exposures and the middle position being a "long" exposure. The "short" exposures are kept to doses <20 mJ/cm^2 to obtain the linear absorption coefficient, while the "long" exposure is used for bleaching measurements and the total dose is adjusted based on the resist material.

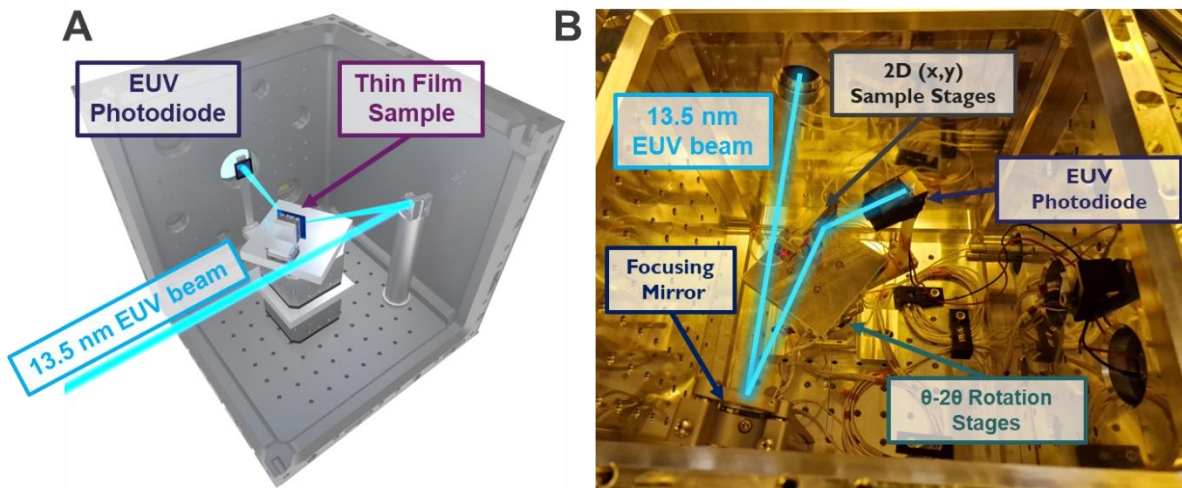## 2.3 AttoLab's Actinic EUV Reflectometry Endstation

Figure 2. (A) Schematic of the actinic reflectometry endstation in AttoLab. (B) Photograph of the main chamber of the reflectometer, showing EUV beam path (blue), focusing mirror, sample stages, and detector.

AttoLab's actinic reflectometry endstation is installed on a separate branch of the spectroscopy beamline and is depicted in Figure 2. The entire endstation is comprised of two-independent vacuum chambers; one for monochromatization and beam routing of the broadband EUV light from the HHG system (not shown) and another for housing the reflectometry apparatus (Figure 2). The first chamber contains a periscope comprised of two MoSi multilayer

mirrors for isolating the 13.5 nm portion of the comb-like spectrum emitting from the HHG system, as well as for steering the beam into the experimental chamber. The experimental chamber houses an additional MoSi mirror for focusing the beam onto the sample (f=10 cm) as well as a pair of high-resolution rotation stages arranged in a θ-2θ geometry. An additional pair of linear translation stages is placed on top of the rotation stages to enable precise positioning and for isolating regions of interest on the sample. The specularly reflected EUV light from the sample is collected by an EUV-sensitive photodiode (AXUV100G, OptoDiode) as a function of the grazing incidence angle. This configuration enables reflectivity measurements over a grazing angle range of ~3-86° with a resolution of 0.05°. Fits to the experimentally obtained reflectivity data are obtained by employing a model of the material system that depends upon the density, thickness, and roughness/intermixing of each layer in the sample. Fitting is performed in IMD software (v5.04) [17] using a Levenberg-Marquandt χ^2 minimization algorithm.

2.4 Sample Preparation and Characterization

2.4.1 Photoresist preparation and characterization

Photoresist samples were prepared via spincoating of the stock solutions. A modified version of the environmentally stable chemically amplified photoresist (ESCAP) was provided by FujiFilm. The composition of the modified ESCAP material was as follows: a backbone polymer of p-hydroxystyrene (48 mol%) and tert-butyl methacrylate (52 mol%), (4-Methylphenyl) diphenyl sulfonium nonaflate as the photoacid generator (17.3 wt%), and trioctylamine as the quencher (7.1 wt%). Commercially available photoresists polymethylmethacrylate (PMMA) and hydrogen silsesquioxane (HSQ) were obtained from AllResist GmbH and used as received. For reflectometry measurements, photoresists were spincoated onto blank Si wafer coupons (2 cm x 2 cm) with only the native oxide layer present (i.e., no underlayer). For radiometry measurements, photoresists were coated onto 50-nm-thick Si_3N_4 membranes (1 mm x 1 mm window size, Norcada Inc.) using a specialized chuck that allows for direct coating on the membranes without backside leakage. In all photoresist samples, the thickness of the photoresist was determined by fitting reflectance curves from a commercial spectroscopic ellipsometer (RC2, JA Woollam Company). In order to achieve high quality fits, blank Si coupons and Si_3N_4 membranes (i.e., with no photoresist) were first measured to determine the thickness of the native SiO_2 and Si_3N_4 layers, respectively. The optical constants from these initial fits were then used in the fitting of the ellipsometry data to obtain thickness values of the photoresists.

2.4.2 Thin film deposition and characterization

Thin films of Ru, TiN, and Nb were prepared for reflectometry measurements on Si wafer substrates. The TiN and Nb samples were prepared in imec's 300 mm cleanroom using standard physical vapor deposition (PVD) processes and calibrated growth times were used to achieve film thicknesses of 30 nm. The Ru sample was prepared at the University of Twente by a similar PVD process using an Ar magnetron-ignited plasma. The thickness of the Ru sample was controlled by a pre-calibrated growth time to 50 nm. Samples were kept in an N_2 glove box prior to measurement to reduce the rate of formation of oxide and contamination layers on the surface.

3.   RESULTS AND DISCUSSION

3.1 Actinic Absorption Measurements on Model Photoresists

The actinic, linear absorption coefficient (α) of a photoresist can provide useful information on the efficiency of the resist to absorb EUV light, which in turn may be linked to electron generation and sensitivity. Measurement of the linear absorption coefficient is readily obtained by measuring the transmission (T) of a photoresist of a given thickness, d,

$$T = e^{-\alpha d} \rightarrow \alpha = -\frac{1}{d}\ln\frac{I}{I_0} \tag{1}$$

where I_0 and I are the incident and transmitted EUV intensity through the resist.

In addition to their linear absorption properties, photoresists can also exhibit dynamic absorption (i.e., "bleaching") as the EUV dose is increased beyond the dose-to-clear limit. For the case of EUV resists, this bleaching phenomenon is caused by the desorption of ligands and release of volatile components during the exposure process. While originally developed to describe photobleaching in deep UV (DUV) resist platforms, the Dill parameters [18] can be used to describe

the bleaching of EUV photoresists despite the different mechanisms underlying DUV and EUV photoresist bleaching. The Dill parameters provide critical input for lithographic modelling and are given in Eqs. 2-4 in their familiar ABC form.

$$A(\mu m^{-1}) = \frac{1}{d} \ln\left(\frac{I(t_{exp})}{I(t_0)}\right) \tag{2}$$

$$B(\mu m^{-1}) = -\frac{1}{d} \ln\left(\frac{I(t_{exp})}{I_0}\right) \tag{3}$$

$$C\left(\frac{cm^2}{mJ}\right) = \frac{A+B}{AI_0 T(0)[1-T(0)]} \left.\frac{dT}{dt}\right|_{t=0} \tag{4}$$

In Eqs. 2-3, d is the photoresist thickness, I_i is the transmitted light intensity through the resist at initial times (t_0) or after the resist has been fully exposed and no further bleaching is observed (t_{exp}). The Dill C parameter (Eq 4) is determined from the extracted A and B parameters, as well as the incident light intensity impinging on the resist (I_0), the transmission at zero exposure time, $T(0)$, and the derivative of the transmitted photon flux at t=0. These parameters can be extracted by fitting the experimental absorbance as a function of EUV dose, which is shown for two model resist systems, PMMA and ESCAP, in Figure 3.
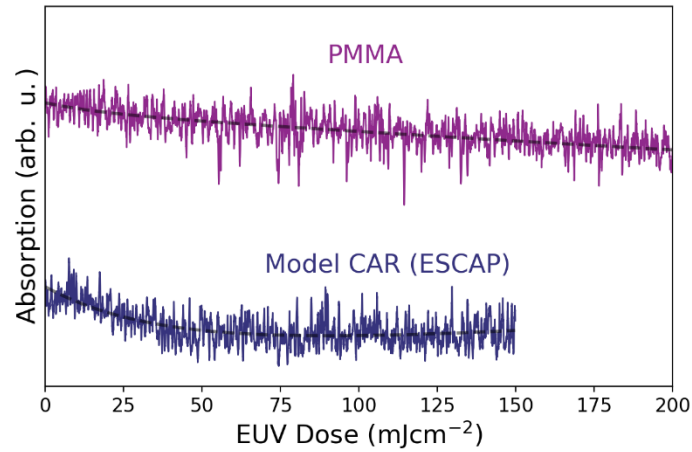

Figure 3. Dynamic 13.5 nm EUV absorption measurements on the model resists PMMA and ESCAP, showing clear bleaching signals as a function of increasing dose. A biexponential fit to the raw data is shown via the dashed line, which is used to determine the Dill A and B parameters. The C parameter is determined by a separate fit at early times to extract $\left.dT/dt\right|_{t=0}$.

The retrieved Dill parameters for PMMA and a model ESCAP resist are given in Table 1. The values for PMMA agree well with previously published results obtained at a synchrotron beamline [7]. However, we observe a significantly lower value for the Dill C parameter, which could be due to the lower light intensity used in our measurements, which decreases the rate of outgassing of CO_2 molecules from the PMMA film. However, we note that further studies on different photoresist formulations are needed to verify this observed difference in Dill C parameter between synchrotron measurements and those made with lower average power sources. Unfortunately, literature values for the ESCAP material are currently not available and thus prevent a direct comparison to previous measurements; however, our extracted values agree well with values typically found for CAR resists without an EUV sensitizer [7]. As such, the compact and accessible radiometry endstation in AttoLab brings not only synchrotron-like capabilities to an accessible laboratory, but also shows the utility of table-top HHG-based EUV sources for photoresist research and development.

Table 1. Extracted Dill parameters for model photoresist systems, PMMA and ESCAP.

Resist	α (um⁻¹)	Dill A (µm⁻¹)	Dill B (µm⁻¹)	Dill C (cm²/mJ)
PMMA	5.43 (5.79)[a]	0.025 (0.02)[a]	6.176 (5.765)[a]	0.031 (0.220)[a]
ESCAP	4.33	1.309	3.373	0.058

[a]Ref. [7].

3.2 Actinic EUV Reflectometry of Thin Film Systems

The EUV reflectivity of thin film systems is largely determined by the associated optical parameters of each layer into which the EUV light can penetrate. The optical parameters in this spectral range define the complex refractive index, which is typically expressed in the familiar δ and β form,

$$\tilde{n}(\omega) = n(\omega) + ik(\omega) = 1 - \delta(\omega) + i\beta(\omega) \tag{5}$$

where $n = 1-\delta$ is the dispersive contribution to the refractive index, $k = \beta$ describes the absorptive component, and we have made explicit the frequency dependence of these parameters. Additionally, the absorption coefficient can be directly calculated from the absorptive component, β,

$$\alpha = \frac{4\pi}{\lambda}\beta \tag{6}$$

where λ is the illuminating wavelength, typically expressed in µm. EUV reflectometry measurements can be used to determine the optical constants of each layer in a sample, by performing a model-based fit of the experimental data that also considers material properties (e.g., density, thickness, and roughness/diffusion).

In order to commission the actinic EUV reflectometer in AttoLab, we have performed reflection measurements on model thin film systems and derive optical, as well as structural, properties from the experimentally obtained reflectivity data. Actinic reflectivity curves for model thin films of Ru, TiN, and Nb are shown in Figure 4, along with corresponding fits that are optimized by adjusting properties of the material system. Despite the lower flux of our EUV source compared to synchrotron sources (and the use of p-polarization), we can measure reflectivity up to grazing angles of 30°-45°, which provides enough data points for fitting of crucial material parameters such as density and film thickness. Additionally, our reflectivity measurements also exhibit a low degree of fluctuation, especially in the low grazing angle range, which is a direct result of the high stability of our tabletop EUV source. Note that for these first commissioning tests, we do not employ lock-in detection or photon referencing techniques to improve the signal-to-noise and detection limit; however, these upgrades are currently being evaluated and will be installed in future iterations of the reflectometry endstation.
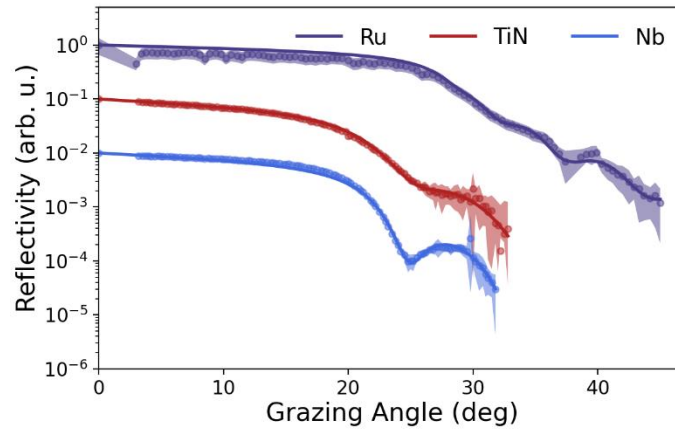

Figure 4. Actinic (13.5 nm) EUV reflectivity spectra of model thin films samples of Ru, TiN, and Nb. The grazing angle is defined as the angle between the incoming EUV beam and the surface. The symbols mark the experimental data points, while the shaded regions around each curve represent the 95% confidence interval of the measured data. Fits to the experimental data are shown via a solid line. The curves have a vertical offset for clarity.

To extract material and optical properties for the systems in Figure 4, we utilize the commercial software IMD [17] in combination with a physical model of each system that considers surface contamination/oxidation, as well as interface formation and layer mixing (if present). As the presence of oxide and interfacial layers can vary depending on the material system, we choose these three model systems as they each represent a category of materials where a) no oxide and intermixing is expected (TiN), b) only oxidation of the surface is expected (Nb), and c) where oxidation and interfacial layer formation are known to occur (Ru) [2,19]. In Table 2 we show the results of the fitting for these 3 model systems. In the case for Ru, we observe the presence of oxidation and intermixing layers that we find necessary to include in order to fit the experimental data. Also, we retrieve optical constants for the Ru layer that match very closely with recent results

from spectroscopic EUV reflectometry measurements performed on a dedicated synchrotron beamline [1], which gives a high degree of confidence in the retrieved values from our measurements. Unfortunately, literature values are not available for many of the optical parameters determined in these systems, but we find reasonable agreement with values estimated from the CXRO database [11]. We note; however, the optical parameters of compounds (e.g., RuO_2, $RuSi_2$, Nb_2O_5) show a lower degree of agreement with predicted values, which is expected as the simulated values are composed of summing the atomic optical properties, rather than the properties of the compound itself. Finally, we note that a rather large oxide layer is observed for the Nb sample, which requires further measurement and analysis to verify.

Table 2. Material properties and optical constants of thin film systems Ru, TiN, and Nb

Material		Density, ρ (g/cm^3)	Thickness (nm)	Roughness/Diffusion (nm)	n	k
"50nm" Ru Film	RuO_2	6.78	2.6	1.05	0.896 (0.943)[a]	0.0245 (0.0214)[a]
	Ru	11.86	46.2	0.22	0.888 (0.888)[b]	0.0169 (0.0154)[b]
	$RuSi_2$	7.58	2.8	0.74	0.935 (0.954)[a]	0.0044 (0.010)[a]
"30nm" TiN Film	TiN	5.47	28.8	1.95	0.935 (0.953)[a]	0.0191 (0.0193)[a]
"30nm" Nb Film	Nb_2O_5	4.30	9.5	0.27	0.952 (0.932)[a]	0.0134 (0.0258)[a]
	Nb	9.27	19.5	0.678	0.927 (0.938)[a]	0.0054 (0.0053)[a]

[a]Ref. [11]
[b]Ref [1].

3.3 Actinic Reflectometry on Model Photoresist Materials

The optical properties of photoresist materials are critical for their lithographic performance and accurate values for optical constants not only aid in simulations, but also give feedback to improve resist performance by engineered design. The recent advances in EUV reflectometry [3,4,15] on resist materials have shown this as a promising technique for extracting actinic optical properties, including sensitivity to exposed/unexposed regions [3]. In Figure 5, we show the actinic reflectivity curves of three model resist systems on a Si substrate.
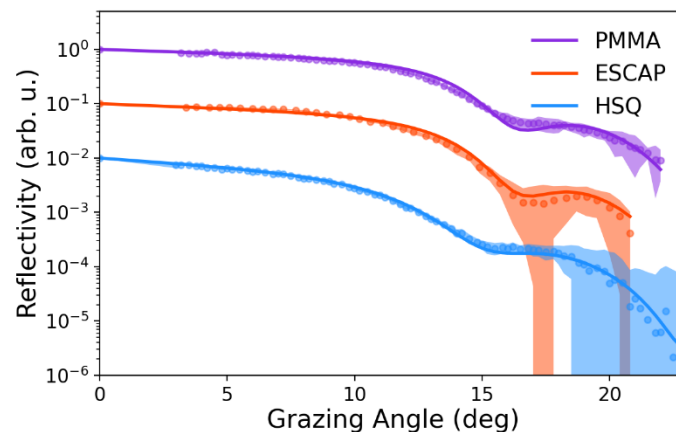

Figure 5. Actinic (13.5 nm) EUV reflectivity spectra of model photoresist systems; PMMA, ESCAP, and HSQ. The grazing angle is defined as the angle between the incoming EUV beam and the surface. Symbols mark the experiment data points, while the shaded regions around each curve represent the 95% confidence interval of the measured data. Fits to the experimental data are shown with a solid line. The reflectivity curves are offset for clarity.

Due to the lower reflectivity of the substrate, the reflectivity data is limited to relatively shallow grazing angles, which limits the spectral features for fitting. To increase the accuracy of the fit from the limited experimental data, we constrain parameters of the photoresist film (e.g., thickness, roughness) using values obtained from spectroscopic ellipsometry on the same sample. This allows for an accurate fit of the experimental data despite the high noise in the region >15° grazing angle. Employing this constraint enables accurate retrieval of density and *n/k* values, which are shown in Table 3. The comparison to literature values is quite good, indicating a high level of confidence in the extracted parameters despite the limited grazing angle range in these preliminary measurements.

Table 3. Extracted material and optical properties of model photoresists.

Resist	density, ρ (g/cm^3)	n	k	α (um^{-1})
PMMA	1.28 (1.18)[a]	0.973	0.00563 (0.00587)[a]	5.24 (5.46)[a]
ESCAP	1.37	0.975	0.00461	4.29
HSQ	1.31	0.980	0.00698 (0.00763)[b]	6.49 (7.11)[b]

[a]Ref [15]
[b]Ref [7]

The main limitation of measuring photoresist samples using a lab-based EUV reflectometer is the lower reflectance of the Si substrate, which places a stricter demand on the required dynamic range for the experiment. However, if the substrate reflectivity can be increased, larger grazing angles can be observed (for a given dynamic range) which provides access to thinner films. Additionally, if a substrate with a large density contrast is used, additional, sharp structures can manifest in the reflectivity spectrum. For instance, Ru has a stronger EUV reflectivity than Si, while also providing a large density compared to typical photoresists. In Figure 6, we compare the simulated reflectivities of a PMMA film coated on a Si or Ru substrate as a function of thickness and grazing angle. From the simulations, it is clear that the Ru substrate gives a higher reflectivity over a wider grazing angle range while sharper oscillations are also observed.
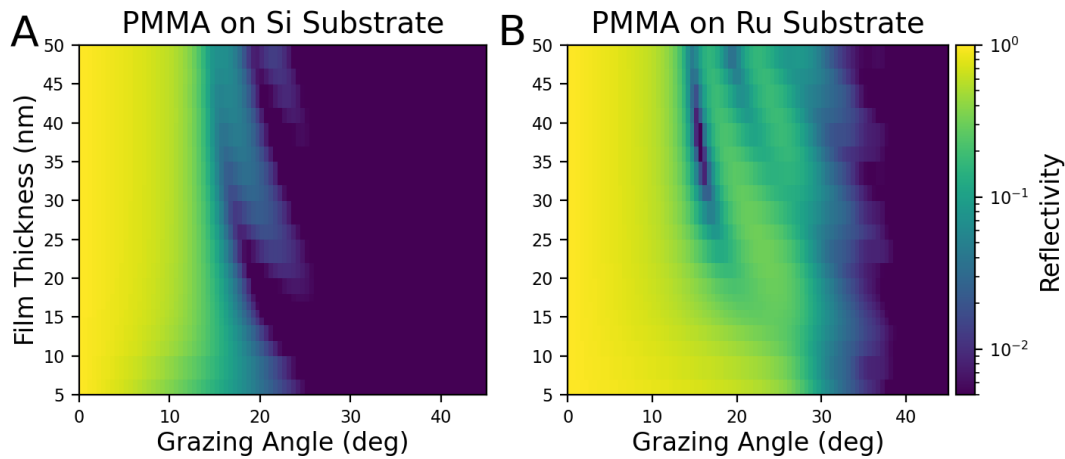

Figure 6. Simulated EUV reflectivity at 13.5 nm of PMMA as a function of grazing angle and thickness on Si (A) and Ru (B) substrates. The Ru substrate results in an enhanced reflectivity as well as adding structures to the reflectivity spectra, which aid in constraining the fit. Simulations are computed using parameters obtained from the CXRO database [11].

To this end, we have explored Ru as a substrate for enhancing the signals in our reflectometer. In Figure 7, we show the experimental results of the reflectivity of PMMA films on Si and Ru substrates. The most striking feature of the reflectivity curves is the extended angular range, which is nearly doubled for the PMMA films on Ru. This enables the measurement of reflectivity curves with a low error for a film thickness of <20nm. Second, the density contrast indeed manifests as additional structures in the reflectivity curve, which is observed as a strong dip after the critical angle.
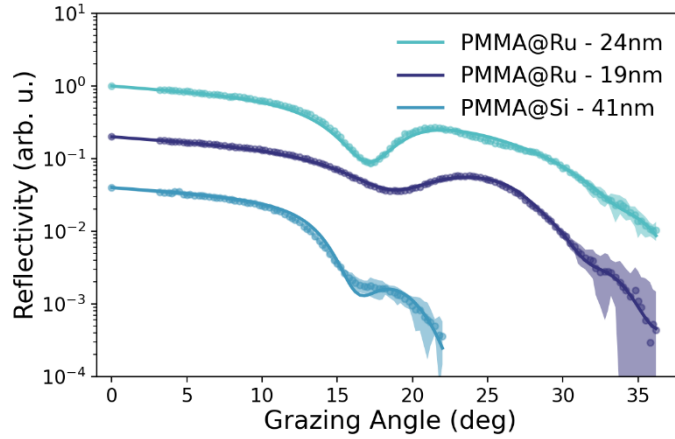
Figure 7. Experimental actinic (13.5 nm) EUV reflectivity spectra of PMMA on Si and Ru substrates. The Ru substrate significantly extends the detectable grazing angle range, enabling measurement of thinner films than would be possible on a Si substrate. The symbols mark the experimental data points while the shaded regions depict the 95% confidence interval of the measured reflectivity. Fits to the experimental data are shown as solid lines. Reflectivity curves are offset for clarity.

While these additional features can help to constrain the fitting process, the introduction of a Ru substrate creates a larger parameter space resulting in less unique solutions. Therefore, we used extracted parameters of an independent measurement of the same bare Ru substrate to limit the parameter space to only those of the resist itself. Results of the fitting are shown in Table 4, with a comparison to those obtained on a standard Si substrate. The retrieved values agree well between the two substrates, with perhaps a slight downward trend in density and extinction coefficient, however more experimentation is required to confirm the observed trend. Nonetheless, these measurements showcase a relatively simple alternative to increasing experimental signals without significantly altering the optical properties of the photoresist.

Table 4. Extracted material and optical properties of PMMA on Si and Ru substrates

Resist	density, ρ (g/cm^3)	Thickness (nm)	n	k	α (um^{-1})
PMMA on Si	1.28 (1.18)[b]	41.5 (41.3)[a]	0.973	0.00563 (0.00587)[b]	5.24 (5.46)[b]
PMMA on Ru	1.25 (1.18)[b]	24.1 (25.1)[a]	0.973	0.00559 (0.00587)[b]	5.20 (5.46)[b]
PMMA on Ru	1.23 (1.18)[b]	19.2 (19.2)[a]	0.973	0.00547 (0.00587)[b]	5.07 (5.46)[b]

[a]Spectroscopic ellipsometry measurements.
[b]Ref. [15], on Si substrate.

4. CONCLUSION

In conclusion, we have demonstrated the power of lab-scale EUV radiometry and reflectometry for the characterization of optical and structural properties of EUV materials. In the case of radiometry, we have realized a flexible, actinic exposure chamber that delivers high-flux, stable EUV light for measuring the static and dynamic absorption properties of photoresists, enabling the extraction of critical absorption parameters. For EUV reflectivity, we have shown a versatile, small-footprint experimental chamber that is well-suited for measuring the optical properties of hard and soft condensed matter systems. These endstations have been benchmarked with measurements on model material systems and comparison to values obtained from synchrotron measurements has validated these techniques for EUV material characterization. Moreover, our results show the utility of tabletop EUV sources based on HHG for EUV material inspection. These new capabilities realized in imec's AttoLab will help to accelerate learning cycles of EUV materials related to photoresists, pellicles, underlayers, masks, and imaging materials.

ACKNOWLEDGEMENTS

REFERENCES

[1] Ciesielski, R. Saadeh, Q., Philipsen, V. Opsomer, K., Soulié, J.-P., Wu, Meiyi, Naujok, P., van der Kruijs, R. W. E., Detavernier, C., Kolbe, M., Scholze, F., Soltwisch, V. "Determination of optical constants of thin films in the EUV" Appl. Opt. **61**, 2060-2078 (2022).

[2] Saadeh, Q., Naujok, P., Philipsen, V., Hönicke, P., Laubis, C., Buchholz, C., Andrle, A., Stadelhoff, C., Mentzel, H., Schönstedt, A., Soltwisch, V., Scholze, F. "Time-frequency analysis assisted determination of the ruthenium optical constants in the sub-EUV spectral range 8 nm – 23.75 nm" Opt. Express **29**, 40993-41012 (2021).

[3] Schröder, S. Bahrenberg, L. Lüttgenau, B., Glabisch, S., Brose, S. Danylyuk, S., Stollenwerk, J., Loosen, P., Holly, C. "Latent image characterization by spectroscopic reflectometry in the extreme ultraviolet" J. Micro/Nanopattern. Mater. Metrol. **21**, 021208 (2022).

[4] Ohta, Y. Sekiguchi, A., Harada, T., Watanabe, T. "The measurement of the refractive index n and k value of the EUV resist by EUV reflectivity measurement method" J. Photopolym. Sci. Technol. **34**, 105-110 (2021).

[5] Philipsen, V. Hendrickx, E., Jonckheere, R. Davydova, N., Fliervoet, T., Neumann, J.-T. "Actinic characterization and modeling of the EUV mask stack" Proc. SPIE **8886**, 29th European Mask and Lithography Conference, 88860B (2013).

[6] Krawk, Y.-J., Bravo-Vasquez, J. P., Chandhok, M., Cao, H., Deng, H., Gullikson, E., Ober, C. K. "Absorbance measurement of polymers at extreme ultraviolet wavelength: Correlation between experimental and theoretical calculations" J. Vac. Sci. Technol. B **24**, 1822-1826 (2006).

[7] Fallica, R., Stowers, J. K., Grenville, A., Frommhold, A. Robinson, A. P. G., Ekinci, Y. "Dynamic absorption coefficients of CAR and non-CAR resists at EUV" Proc. SPIE **9776**, Extreme Ultraviolet (EUV) Lithography VII, 977612 (2016).

[8] Fallica, R., Haitjema, J., Wu, L., Castellanos, S., Brouwer, F., Ekinci, Y. "Absorption coefficient and exposure kinetics of photoresists at EUV" Proc. SPIE **10143** Extreme Ultraviolet Lithography VIII, 101439A (2017).

[9] Shehzad, A., Vesters, Y., De Simone, D., Pollentier, I., Nannarone, S. Vandenberghe, G. De Gendt, S. "Photoresist absorption measurement at extreme ultraviolet (EUV) wavelength by thin film transmission method" J. Photopolym. Sci. Technol. **32**, 57-66 (2019).

[10] Manouras, T., Argitis, P. "High Sensitivity Resists for EUV Lithography: A Review of Material Design Strategies and Performance Results" J. Nanomater. **10**, 1593 (2020).

[11] Henke, B. L., Gullikson, E. M., Davis, J. C. "X-ray interactions: photoabsorption, scattering, transmission, and reflection at E=50-30000 eV, Z=1-92" Atomic Data and Nuclear Data Tables, **54**, 181-342 (1993).

[12] Delmotte, F., Burcklen, C., Alameda, J., Salmassi, F., Gullikson, E., Soufli, R. "New method for the determination of photoabsorption from transmittance measurements in the extreme ultraviolet" Opt. Express **30**, 23771-23782 (2022).

[13] Wu., M., de Marneffe, J.-F., Opsomer, K., Detavernier, C., Delabie, A., Naujok, P., Caner, Ö., Goodyear, A., Cooke, M., Saadeh, Q., Soltwisch, V., Scholze, F., Philipsen, V. "Characterization of Ru(4-x)Ta(x) (x=1,2,3) alloy as material candidate for EUV low-n mask" Micro. Nano. Eng. **12**, 100089 (2021).

[14] Wu, M., Thakare, D., de Marneffe, J.-F., Jaenen, P., Souriau, L., Opsomer, K., Soulié, J.-P., Erdmann, A., Mesilhy, H., Naujok, P., Foltin, M., Soltwisch, V., Saadeh, Q., Philipsen, V. "Study of novel EUVL mask absorber candidates" J. Micro/Nanopattern. Mater. Metrol. **20**, 021002 (2021).

[15] Kostko, O., McAfee, T. R., Ma, J., Blackwell, J. M., Naulleau, P. "Experimental characterization of model resist materials" Proc. SPIE **11854** International Conference on Extreme Ultraviolet Lithography 2021, 1185407 (2021).

[16] Holzmeier, F., Dorney, K., Larsen, E. W., Nuytten, T. Singh, D. P., van Setten, M., Vanelderen, P., Bargsten, C., Cousin, S. L., Raymondson, D., Rinard, E., Ward, R., Kepteyn, H., Böttcher, S., Dyachenko, O., Kremzow, R., Wietstruk, M., Pourtois, G., van der Heide, P., Petersen, J. "Introduction to imec's AttoLab for ultrafast kinetics of EUV exposure processes and ultra-small pitch lithography" Proc. SPIE **11610**, Novel Patterning Technologies, 1161010 (2021).

[17] Windt, D. L. "IMD – Software for modeling the optical properties of multilayer films" Comput. Phys. **12**, 360 (1998).

[18] Dill, F. H., Hornberger, W. P., Hauge, P. S., Shaw, J. M. "Characterization of positive photoresist" IEEE Transactions on Electron Devices **ED-22**, 445-452 (1975).

[19] Wood, O., Wong, K., Parks, V., Kearney, P., Meyer-Ilse, J., Luong, V., Philipsen, V., Faheem, M., Liang, Y., Kumar, A., Chen, E., Bennett, C., Fu, B., Gribelyuk, M., Zhao, W., Mangat, P., Van der Heide, P. "Improved Ru/Si multilayer reflective coatings for advanced extreme-ultraviolet lithography photomasks" Proc. SPIE **9776** Extreme Ultraviolet (EUV) Lithography VII, 977619 (2016).